Magneto-electroluminescence study of fringe field in 'magnetic' organic light emitting diodes

Xiaojie Liu¹, Ashish Chanana^{1,2}, Haoliang Liu¹, Jingying Wang¹, Ohyun Kwon³*, Byoungki Choi³, Sunghan Kim³, and Z, Valy Vardeny¹*

Abstract

Magneto-electroluminescence (MEL) represents the electroluminescence intensity change upon the application of an external magnetic field. We show that the MEL field response in 'magnetic' organic light emitting diodes, where one electrode is ferromagnetic (FM), is a powerful technique for measuring the induced fringe field, \vec{B}_F from the FM electrode into the organic layer. We found that the in-plane fringe field, $\vec{B}_{F||}$ from 3 nm Co and Ni₈₀Fe₂₀ FM electrodes is proportional to the applied field, $\vec{B}_{||}$. The fringe field of 3 nm Ni₈₀Fe₂₀ film was also investigated for an applied out-of-plane magnetic field, \vec{B}_{\perp} . We found that the out-of-plane fringe field has two components; a component that is parallel or antiparallel to \vec{B}_{\perp} and remains unchanged with the distance, d from the FM electrode. Whereas the other component is highly inhomogeneous, parallel to the surface and steeply decreases with d. We show that the obtained \vec{B}_F is independent of the underlying mechanism for the MEL(B) response, and thus may be considered as universal.

1. Introduction

Magnetic thin films have attracted substantial scientific and technological interest because of their wide applications in spintronics^{1,2}, high frequency devices³, magnetic sensors^{4,5}, data storage media⁶ and read heads⁷. The magnetic properties of thin ferromagnetic (FM) films have been studied under diverse conditions such as different temperatures, applied magnetic field direction and strength.² However, so far there has been no accurate method for measuring the fringe field from thin FM films. Fringe field is the peripheral magnetic field emanating from a ferromagnet or magnet core⁸. Usually the fringe field has been simulated using magneto-statics

¹ Department of Physics & Astronomy, University of Utah, Salt Lake City, Utah 84112, USA

² Department of Electrical and Computer Engineering, 50 S. Central Campus Drive, University of Utah, Salt Lake City, UT 84112, USA

³ Samsung Advanced Institute of Technology, Samsung Electronics Co., Ltd. 130, Samsung-Ro, Youngtong-Gu, Suwon-Si, Republic of Korea, 16678 **Keywords**: Fringe filed, ferromagnetic films, magneto-electroluminescence, OLED, TADF, Alq₃.

models in relation to magnetization measurements.⁸ Although magnetic force microscopy (MFM) has been successfully used for measuring the fringe field perpendicular to the FM films, this method does not accurately determine the fringe field strength parallel to the FM substrate.^{9,10}

Meanwhile the magnetic field effect (MFE) has been successfully used for studying spin-dependent processes in organic semiconductors and organic-inorganic hybrid perovskites based films and devices, including solar cells and light emitting diodes¹¹⁻¹⁴. The MFE underlying processes are based on magnetic field modification of spin-dependent reactions that may be measured by photoluminescence, electroluminescence (EL), photocurrent, photoinduced absorption and conductivity. In particular, magneto-EL (MEL) is a very useful tool for studying the spin dependent light-emitting processes that control the EL intensity and emission color in organic light emitting diodes (OLEDs). ^{14,15}

Engineered fringe field was first mentioned in MFE response of Alq₃-based OLED having structured FM electrode.⁸ Subsequently, magnetic fringe field control of the MFE response in OLEDs have been studied using different FM films¹⁶⁻²⁰. Spatially inhomogeneous magnetic fringe

field was believed to be responsible for these phenomena. Ref [20] dubbed this mechanism as ' Δ

B mechanism'. Inspired by these previous works it is clear that further studies of the magnetic fringe field in OLEDs using the MEL technique are in order.

In this work we have used the MEL(B) response in 'magnetic' OLEDs based on thin FM electrodes as cathodes, to systematically study the fringe field. The MEL(B) response in traditional OLED is independent of the direction of the external magnetic field (\vec{B}_E). The response is usually a monotonic function of the external field (B_E), which can be fitted empirically using Lorentzian or non-Lorentzian functions.²¹ The main idea for studying fringe fields by the MEL(B) response in magnetic OLEDs is that when a fringe field (\vec{B}_F) is induced in the active layer by the FM electrode, then B_E needs be replaced with the local magnetic field, \vec{B}_L such that:

$$\vec{\mathbf{B}}_L = \vec{\mathbf{B}}_F + \vec{\mathbf{B}}_E. \tag{1}$$

Consequently, by comparing MEL(B_E) response of a traditional OLED with that of a magnetic OLED, we may determine \vec{B}_F using Eq.(1).

In this work we have used different types of OLED devices, where the active materials are Alq_3 or thermally activated delayed fluorescence (TADF) compounds. It has been known that the MEL(B) response in Alq_3 -based OLEDs is caused by the hyperfine interaction of polaron pairs^{21,22}, whereas the MEL(B) response in TADF-based OLEDs is believed to be dominated by the Δg mechanism of the exciplex state¹⁵. With these two different types of OLEDs, we show here that the fringe field obtained from the MEL(B) response is *independent* of the MEL underlying processes, and thus the method introduced here is universal²³. We also show that this method is viable for different types of ferromagnetic films, and of various thicknesses. We analyze the induced fringe field in two typical conditions, with \vec{B}_E parallel (in-plane) or perpendicular (out-of-plane) to the FM electrode plane.

Since there are about eight types of different OLED devices discussed in this work, then for the reader benefit Table 1 summarizes the purpose and device structure of all OLEDs used in our work. There are OLEDs based on TADF or Alq3 organic active layers; traditional devices; and magnetic devices based on NiFe ferromagnetic cathode with various thicknesses.

Table 1: Summary of the purpose and structure of all OLED devices presented in this work.

Purpose	Active Material	Device #	Structure
In-plane FF (3 nm FM layer)	TADF (mCP:B3PYMPM)	1	ITO/PEDOT:PSS/TADF (40 nm)/LiF/Al
		2	ITO/PEDOT:PSS/TADF (40 nm)/LiF/Ni ₈₀ Fe ₂₀ (3 nm)/Al
	Alq₃ (Thickness Dependence)	3	ITO/PEDOT:PSS/Alq ₃ (20-140 nm)/LiF/Al
		4	ITO/PEDOT:PSS/Alq ₃ (20-140 nm)/LiF/Ni ₈₀ Fe ₂₀ (3 nm)/Al
	Comparison of Ni ₈₀ Fe ₂₀ and Co		ITO/PEDOT:PSS/Alq ₃ (20 nm)/LiF/Ni ₈₀ Fe ₂₀ (3 nm)/Al
			ITO/PEDOT:PSS/Alq₃(20 nm)/LiF/Co(3 nm)/Al
Out-of-plane FF (3 nm FM layer)	TADF (mCP:B3PYMPM)	5	ITO/PEDOT:PSS/TADF (40 nm)/LiF/Al
		6	ITO/PEDOT:PSS/TADF (40 nm)/LiF/Ni ₈₀ Fe ₂₀ (3 nm)/Al
	Alq₃ (thickness dependence)	7	ITO/PEDOT:PSS/Alq₃(20-140 nm)/LiF/Ni ₈₀ Fe ₂₀ (3 nm)/Al
In-place FF (FM layer thickness dependence)	TADF (MeO-TPD: 3TPYMB)	8	ITO/PEDOT:PSS/TADF/LiF/Ni ₈₀ Fe ₂₀ (0, 3, 5, 30 nm)/Al

2. Results and Discussion

2.1 The OLED devices

Details of the traditional and 'magnetic' device fabrication methods are given in the experimental section. The molecular structures of the active layers such as mCP (TADF donor), B3PYMPM (TADF acceptor) and Alq₃ molecules are shown in Figure 1a. The device structure of the mCP/B3PYMPM based OLED without (device1) and with a 3 nm Ni₈₀Fe₂₀ electrode ('magnetic' device2) are presented in the insets of Figures 1c and 1d. The 40 nm active organic layer in the device is composed of the co-deposited blend of mCP and B3PYMPM with a volume ratio of 1:2. Figure 1b shows the atomic force microscope (AFM) image of the top LiF surface in the multilayer structure comprise of glass/ITO/PEDOT:PSS/mCP:B3PYMPM/LiF. The obtained roughness is a good estimate for the inhomogeneous shape of the 3 nm Ni₈₀Fe₂₀ surface. Figures 1c and 1d depict the I-V and EL-V characteristic responses of device1 and device2 in semi-logarithmical

y-axis. The approximately straight lines at high applied bias voltage indicate the exponential nature of the current-voltage relation in both devices.

We note that the 'magnetic' device2 has a higher turn-on voltage than the traditional device1, because of the higher work function of $Ni_{80}Fe_{20}$ compared with that of aluminum (Figure S5). This may be also deduced from the turn-on current density that is much higher for device2. This indicates that at operation with EL emission, the density of holes is much larger than the electron density. Consequently, the e-h recombination zone of the device is close to the LiF layer, which is subjected to fringe field from the FM electrode, even if the active layer is much thicker than the depth inside the organic layer at which the fringe field exists.

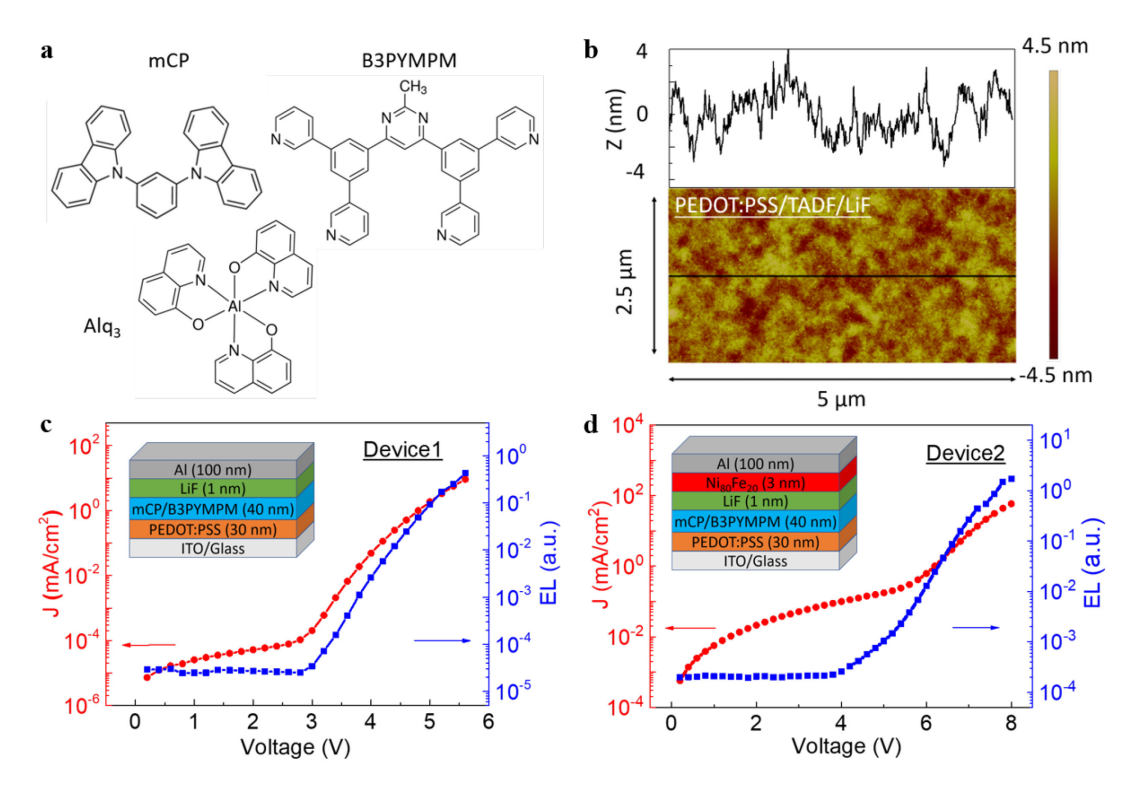


Figure 1. Morphology and physical characterization of the TADF-based OLED devices without (device1) and with a 3 nm Ni₈₀Fe₂₀ electrode ('magnetic' device2). a, The chemical structures of mCP (TADF donor), B3PYMPM (TADF acceptor) and Alq₃ molecules. b, The atomic force microscope (AFM) image of the top LiF surface in a multilayer comprises of glass/ITO/PEDOT:PSS/mCP:B3PYMPM/LiF. The upper section shows the change in height along the black line in the bottom section. c, The I-V (red line) and EL-V (blue line) responses of device1 on logarithmical y-scale. The inset shows the respective device structure. d, Same as in (c) but for device2.

2.2 Application of in-plane external field

Figures 2a and 2b show the MEL(B) responses of device1 and device2, where B is applied parallel to the device plane. The MEL(B) response is defined by the relation:

$$MEL(B) = \frac{[EL(B) - EL(0)]}{EL(0)} \times 100\%,$$
 (2)

where EL(B) [EL(O)] is the EL intensity measured at the external magnetic field, B [or B = 0]. The red

lines in Figures 2a and 2b are fits using a non-Lorentzian function:

$$MEL(B) = MEL_{max} \times \frac{B^2}{(|B|+B_0)^2} , \qquad (3)$$

where MEL_{max} is the MEL(B) where $B \gg B_0$, and B_0 is a fitting constant at which field $MEL(B_0) = MEL_{max}/4$. From the fitting of the MEL(B) responses, the full width at half maximum (FWHMs) were determined to be 18 mT and 60 mT for device1 and device2, respectively. We believe that the larger FWHM in the 'magnetic' OLED is due to the induced fringe field from the FM electrode (see below).

It was proposed ¹⁵ that the ' Δ g mechanism' explains the MFE in TADF donor-acceptor based films and OLEDs, where Δ g is the difference between the g-factors of the electron and hole in the exciplex manifold. Δ g may be large for TADF exciplexes because the electron and hole are separated onto the acceptor and donor molecules, respectively. In this model Δ g increases the spin mixing rate between the singlet exciplex state (¹EX) and triplet exciplex states (³EX), when subjected to an external magnetic field ¹³ due to different precession frequencies of the spin ½ electron and hole. Consequently, this decreases the population of ³EX because of the much shorter life-time of ¹EX compared to that of ³EX. This is the so-called 'magnetic field induced reverse intersystem crossing' (M-RISC) process. ²⁴ The FWHM of the MFE(B) response due to this mechanism is proportional to $1/\Delta g$. ¹³

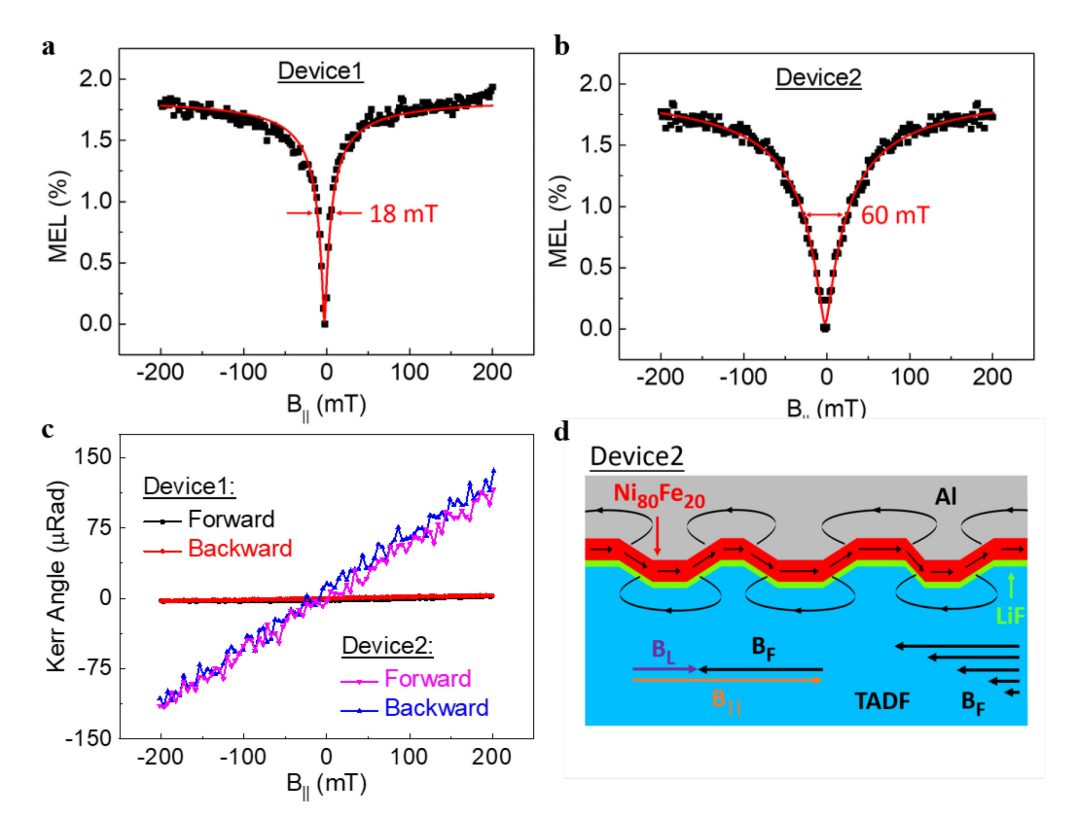


Figure 2. In-plane MEL(B) responses of OLED device1 (traditional) and device2 (having 3 nm thick NiFe electrode), and the mechanism for inducing the in-plane fringe field. a, MEL(B) response of device1 up to 200 mT showing FWHM of ~18 mT. The bias voltage and corresponding current are 6 Volts and 25 mA/cm², respectively. b, Same as in (a) but for device2, having FWHM of 60 mT. The bias voltage and corresponding current are 7.5 V and ~ 25 mA/cm², respectively. c, Magneto-optic Kerr effect (MOKE) measurements of device1 and device2; the latter shows the M(B) response of the 3 nm thick Ni₈₀Fe₂₀ FM electrode. d, Schematics of the local field, B_L that influences the MEL(B) response of

device2 subjected to an externally applied field, B_{\parallel} . B_{F} is the induced fringe field from the FM electrode. The arrows inside the $Ni_{80}Fe_{20}$ layer represent the FM film magnetization. The curved arrows represent the fringe field induced by the magnetic dipoles in the FM. The group of arrows at the right bottom corner represent the decreasing magnitude of the fringe field with increasing distance from the FM layer.

When in proximity to a FM surface electrode, the organic active layer is subjected to a fringe field induced by the substrate magnetization. The $Ni_{80}Fe_{20}$ film does not affect the g-factors of the electrons and holes in the organic layer. Rather, under in-plane external magnetic field $(\vec{B}_{||})$, the FM film magnetization induces an in-plane fringe field (\vec{B}_F) in the active layer, which decays away from the FM electrode, as shown in Figure 2d; where \vec{B}_F is antiparallel to $\vec{B}_{||}$. However we believe that the recombination zone in device2 is close to the LiF layer, and thus the e-h pair are subjected to the fringe field having substantial strength.

According to equation (1) for parallel field vectors, the local field, B_L in the active layer is: $B_L = B_{\parallel}$ -B_F, where B_L, B_{II} and B_F are the correspondent field strengths. As shown in Figure 2c, the Kerr angle measured from the glass side has a linear relationship with the external in-plane magnetic field up to 200 mT. This indicates that the induced fringe field, B_F which is proportional to the FM magnetization, would, in turn, be proportional to B_{||}, leading to a linear relationship between B_| and B_{II}. This conclusion is in agreement with the MEL(B) responses of device1 and device2. The MEL(B) response of device2 has the same shape as that of device1 except that is broader. In this case the calculation of the fringe field (at the recombination zone) is straightforward. The FWHMs ratio of device1 and device2, estimated from the MEL(B) responses is ~0.3, this is equal to the ratio B_L/B_{\parallel} which is $(B_{\parallel} - B_F)/B_{\parallel}$. Consequently we calculate from Eq. (1) $B_f = 0.7 B_{\parallel}$, or B_f =140 \pm 14 mT at applied field $B_{||}$ = 200 mT. We note that in our analysis we did not take into account the strengths of the two MEL(B) responses, because these may depend on many factors. 14,25 However, the FWHM of the MEL(B) response is a more robust property of the MFE response. 13,26,27 We also note that a more accurate measurement of the magnetization upon the application of B_{||} is achieved using the Microsense EZ7 vibrating sample magnetometer (VSM), as shown in Figure S1a. There are two types of in-plane magnetization as shown in Figure S1b. The MOKE technique is more sensitive to the magnetization type ii, which is induced by the roughness of the FM film.

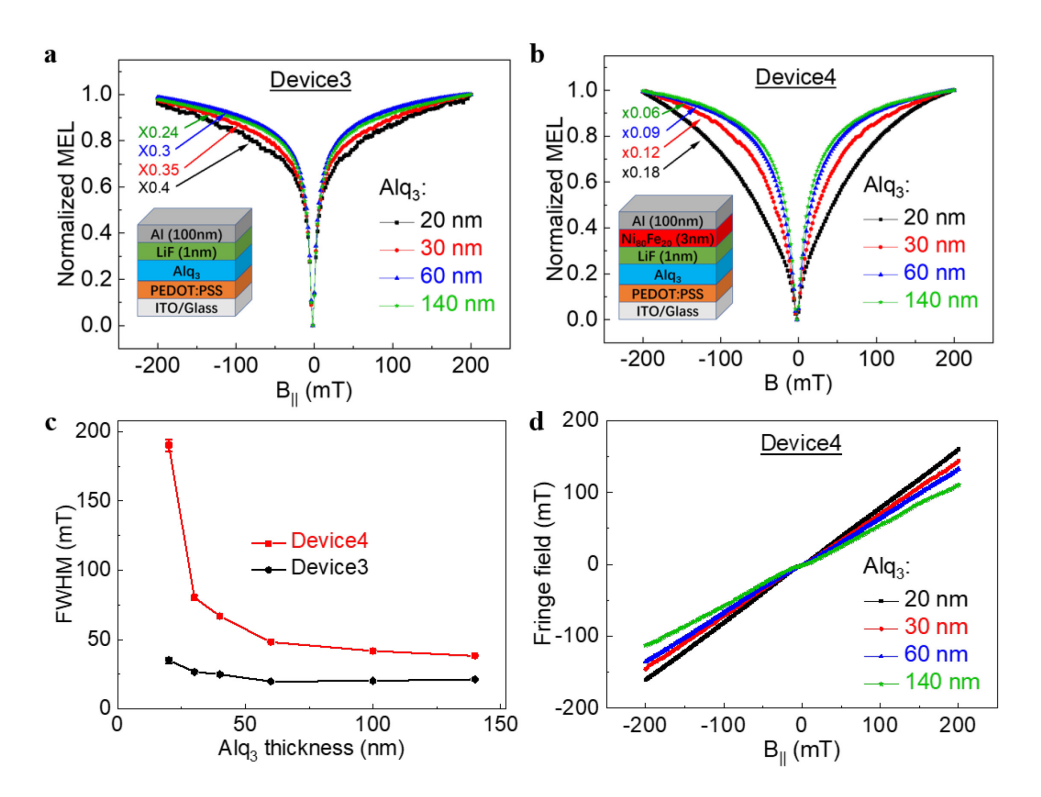


Figure 3. Normalized MEL(B) responses of the Alq₃-based OLEDs without (series device3) and with (series device4) a 3 nm thick Ni₈₀Fe₂₀ electrode and various Alq3 thicknesses. a, MEL(B) responses in series device3 having Alq₃ thickness as given, measured at a fixed current density level of 25 mA/cm². b, Same as in (a) but for series device4. c, FWHM of the MEL(B) responses in series device3 (black curve) and series device4 (red curve) plotted vs. the Alq₃ thickness layer in the device. d, The average fringe field in the Alq₃ layer vs. the external in-plane magnetic field in series device4 that was calculated based on the MEL(B) responses in (a) and (b) [see text].

For comparison, we repeated the MEL measurements on a series of Alq₃-based OLEDs having various organic active layer thicknesses. Figure 3a shows the MEL(B) responses of the Alq₃-based OLEDs (series device3) with different thicknesses, measured at the same current level of 25 mA/cm². The FWHM of the MEL(B) response here exhibits only small change when the active layer thickness increases from 20 nm to 140 nm (Figure 3c). This is because the width of the MEL(B) response is mainly determined by the hyperfine field in the Alq₃ active layer, which is an intrinsic property.²⁷ In addition, Figure S4 shows that in our Alq₃ devices, the FWHM is almost independent of the applied voltage. In contrast, Figure 3b shows that the FWHM of the MEL(B) response in the Alq₃-based magnetic OLEDs having 3 nm Ni₈₀Fe₂₀ electrode (series device4) changes substantially with the Alq₃ thickness. This is because the fringe field decreases with the distance from the FM electrode, and the recombination zone in the device is further from the LiF layer in thicker devices.

Based on our analysis discussed above for TADF-based magnetic OLEDs we can calculate the fringe field at the recombination zone in the active layer of series device4. As shown in Figure 3d, the fringe field is linear function of the external in-plane magnetic field; and decreases with increasing the Alq_3 layer thickness. Interestingly, we calculate the fringe field in a 40 nm Alq_3 layer

to be 142±2 mT at an external magnetic field of 200 mT. This value agrees very well with the fringe field obtained in device2 with TADF (140 mT) that was also 40 nm thick. This agreement emphasizes that the fringe field in the magnetic OLEDs does not depend on the OLED active layer, since it is induced by a process that mostly depends on the FM electrode; and the recombination zone in both devices is close to the LiF layer.

It is worth mentioning that device4 series having thick Alq₃ active layer show an almost constant difference in the FWHM values compared with Device3. We interpret this surprising result that the recombination zone of electrons and holes is not uniformly distributed in the active layer, but rather is close to the LiF layer in all devices. This can be rationalized by the poor electron injection efficiency of the FM electrode in device4 series. Under this imbalanced condition the holes density in the active layer is much higher than the electron density, leading to e-h recombination close to the inefficient cathode. The imbalance injection efficiency of the anode and cathode in device4 series may be deduced from the increase in the turn-on voltage in device4 compared to that of device3, as shown in detail in Figure S2.

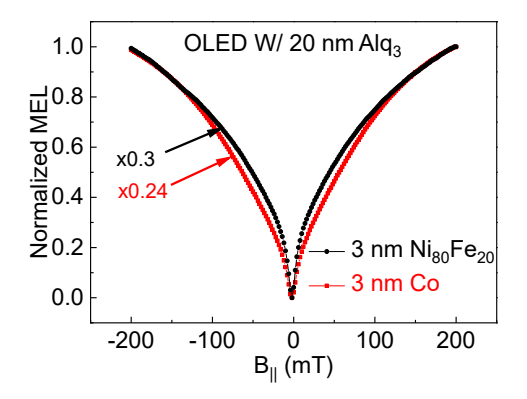


Figure 4. MEL(B) responses of Alq_3 based OLEDs having a 3 nm $Ni_{80}Fe_{20}$ (black) and Co (red) ferromagnetic electrodes. The Alq_3 layer thickness in 20 nm in both devices.

To further explore the in-plane fringe field, we replaced the 3 nm $Ni_{80}Fe_{20}$ film with a 3 nm Co film in a 20 nm Alq_3 -based OLED. In Figure 4 we show the MEL(B) responses of the device with a 3 nm $Ni_{80}Fe_{20}$ electrode compared to that with a 3 nm Co electrode. The larger FWHM of the MEL(B) response in the Co based device indicates that the fringe field of the 3 nm Co film is larger than that of the 3 nm $Ni_{80}Fe_{20}$ film.

2.3 Application of out-of-plane external field

The MFE(B) responses in OLEDs are usually independent of the applied field direction. However, the MEL(B) responses of devices with ferromagnetic electrodes may have angular field dependence because the induced fringe field may be very different for applied field parallel or perpendicular to the FM electrode. In order to study the fringe field at applied field, \vec{B}_{\perp} perpendicular to the FM electrode we measured the MEL(B) responses of both TADF- and Alq₃-based OLEDs for an applied field \vec{B}_{\perp} . To increase the signal to noise ratio in this geometry,

the active layer in the TADF-based OLEDs has been changed to a triple-layer structure of donor/donor-acceptor blend/acceptor; namely: mCP (4nm) / blend (24nm, mCP:B3PYMPM = 1:2) / B3PYMPM (8nm).

Figure 5a shows the MEL(B) responses of traditional device5 and magnetic device6 upon applying \vec{B}_{\perp} . The MEL(B) response of the traditional device5 has the same shape as that when applying an in-plane field (see device1, Fig. 2a); in agreement with the literature. However, the MEL(B) response when applying an out-of-plane field of device6 is very different from its in-plane MEL(B) response (see device2, Figure 2b). Here the low field part (B<100 mT) has the same shape as the non-magnetic MEL(B) response of device5, except with a larger FWHM; this is in fact similar to our measurements using in-plane magnetic field described above. However, the high field part (100<B<200 mT) has a pronounced shoulder that results in a much broader MEL(B) response compared to that of device5.

To understand this finding, the out-of-plane magnetization of the Ni $_{80}$ Fe $_{20}$ electrode in device6 was measured using vibrating sample magnetometer (VSM) apparatus, as shown in Figure 5b. We could fit the magnetization response with a "double error function", as shown in Figure S1b. The low-field component (19%) of the Ni $_{80}$ Fe $_{20}$ film shows a linear response, indicating an easier magnetization response for \vec{B}_{\perp} . The domains structure and size in thin FM thin films have been described in Ref.[9] and Ref[10] using MFM microscopy. When applying an out-of-plane field, it was found that there are three types of domains: domains with in-plane magnetization, those having magnetization parallel to \vec{B}_{\perp} and those with magnetization antiparallel to \vec{B}_{\perp} , as depicted schematically in Figure 5c. To better understand the extend of the resulting three fringe field components when applying \vec{B}_{\perp} , we also measured the thickness dependence of the MEL(B) responses in Alq $_3$ based magnetic OLEDs, as shown in Figure 5d. It is seen that the shoulder component of the MEL(B) response gradually disappears, and is completely gone for the 140 nm device; whereas the "broadening effect" in the MEL(B) response still remains in all devices. Actually, the "broadening effect" does not change much with the Alq $_3$ thickness; which is very different from the case of the in-plane fringe field.

To further study the fringe field when applying \vec{B}_{\perp} , we fitted the MEL(B) response for the 140 nm Alq₃ based magnetic device with a non-Lorentzian function, as shown in the inset of Figure 5d. In this device, we only need to consider the parallel fringe field component that induces the "broadening effect". Subsequently, we have treated the perpendicular fringe field component, \vec{B}_F^{per} as a perturbation term. \vec{B}_F^{per} is uniquely induced by \vec{B}_{\perp} because it does not exist in the case of the in-plane field. Also we assumed that \vec{B}_F^{in} is proportional to the magnetization (M(B)) of the Ni₈₀Fe₂₀ film. We thus fit the VSM measured response, M(B) with a modified error function, $\text{erf}(\mathbf{x})$, where

$$\operatorname{erf}(\mathbf{x}) = \frac{1}{\sqrt{\pi}} \int_{-x}^{x} e^{-t^2} dt.$$
 (4)

$$M(B) = A \times erf(k \times B) \tag{5}$$

The fit is shown in Figure 5b, and the parameter $k = 0.0026 \text{ mT}^{-1}$. Consequently we could fit the MEL(B) response using both parallel and antiparallel components, as detailed in the S.I. section. The fit to the out-of-plane MEL(B) response of device6 is excellent (see Figure 5a).

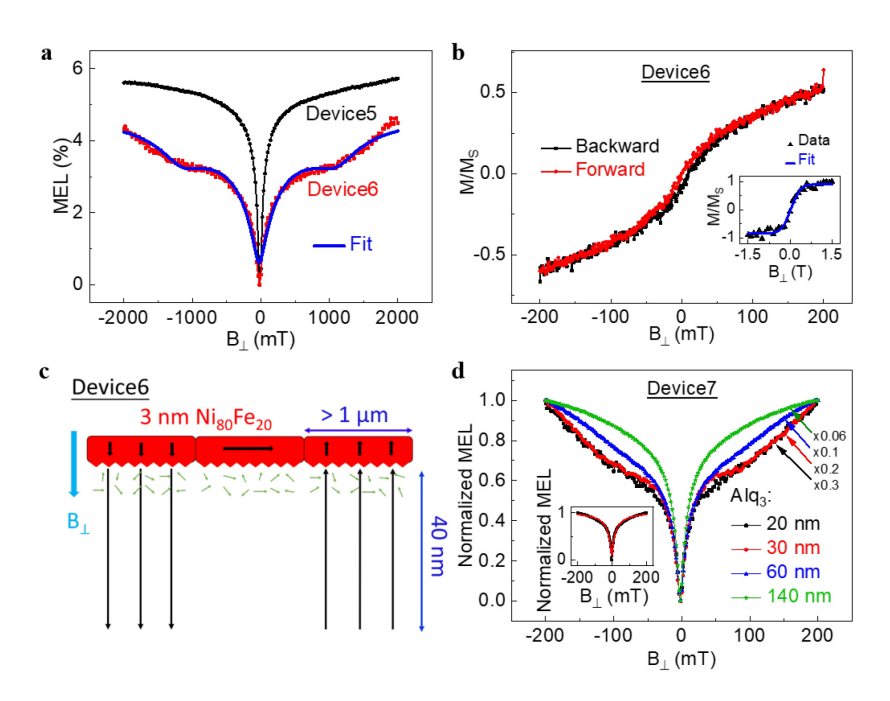


Figure 5. MEL(B) responses in Alq₃-based OLEDs upon application of an out-of-plane field. a, MEL(B) responses of traditional device5 (black line) and 'magnetic' device6 having 3 nm thick NiFe electrode (red line) subjected to an out-of-plane field. The blue line through the data points is a fit (see text and S.I.). **b**, Out-of-plane magnetization of device6 up to 200 mT measured using vibrating sample magnetometer (VSM) apparatus. The inset shows the VSM result measured from -1.5 T to 1.5 T, which is fitted using equation (5). **c**, Schematics of the fringe field in device6 induced by a perpendicular field, B_{\perp} . **d**, Out-of-plane MEL(B) responses of series device7 having various Alq₃ thicknesses, as given. The inset shows the fit (red line) of the MEL(B) response (black points) of 140 nm thick Alq₃ - based device using a non-Lorentzian function; where the FWHM is 43 mT.

2.4 Fringe fields from FM films of different thicknesses

We have also studied the MEL(B) response in 'magnetic' OLEDs with different NiFe thickness, using a solution-based TADF active layer of MeO-TPD/3TPYMB with a weight ratio of 1:4 (device8). Figure 6a shows the chemical structures of MeO-TPD (donor) and 3TPYMB (acceptor). Figure 6b shows the MEL(B) responses of series device8 with different Ni $_{80}$ Fe $_{20}$ electrode thickness, while keeping constant the TADF layer thickness. It is seen that the MEL(B) response narrows with the increasing the Ni $_{80}$ Fe $_{20}$ thickness. This implies that the "average fringe field" in the active layer is smaller for thicker Ni $_{80}$ Fe $_{20}$ film. Specifically, the average fringe field of the 30 nm Ni $_{80}$ Fe $_{20}$ film is negligible, because the MEL(B) responses of the traditional and magnetic device8 series in this case are the same. From the Magneto-static theory it has been established that a thin ferromagnetic film with 'perfect interfaces' cannot induce a fringe field, except near its two magnetic poles. 'Perfect interfaces' here means that the FM film roughness is much smaller than its thickness, as is the case for the 30 nm Ni $_{80}$ Fe $_{20}$ film. In contrast, if the film roughness is comparable to the film thickness, as is the case for the 3nm and 5nm Ni $_{80}$ Fe $_{20}$ devices, there is an induced fringe field close to the surface of the FM film. We thus conclude that this fringe field

understanding is in agreement with our findings.

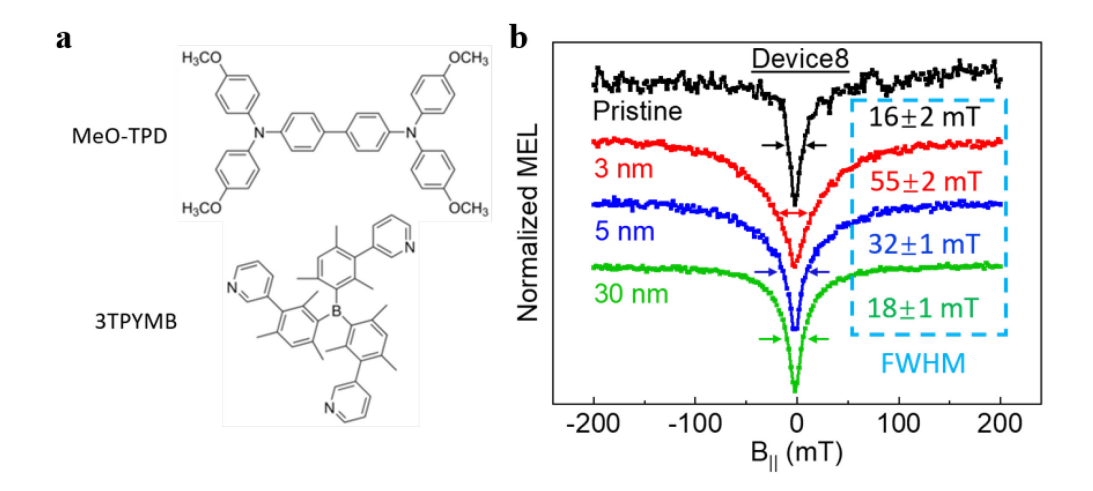


Figure 6. In-plane MEL(B) responses of solution-based TADF magnetic OLEDs with various $Ni_{80}Fe_{20}$ electrode thicknesses (series device8). a, The chemical structures of MeO-TPD (TADF donor) and 3TPYMB (TADF acceptor). b, The MEL(B) responses and corresponding FWHM of series device8 without FM electrode (pristine, black line) and with $Ni_{80}Fe_{20}$ electrodes with various thicknesses, as given.

3. Conclusion

We have shown that the MEL(B) response in 'magnetic' OLED devices is a powerful technique for measuring the fringe field induced by the ferromagnetic electrodes. Specifically we show that the fringe field (\vec{B}_F) of a 3 nm Ni₈₀Fe₂₀ FM electrode subjected to an in-plane magnetic field $(\vec{B}_{||})$ is antiparallel and proportional to $\vec{B}_{||}$; and decreases steeply with increasing distance from the FM electrode. In addition we found that the in-plane \vec{B}_F decreases with increasing the FM electrode thickness; it diminishes completely for a 30 nm thick Ni₈₀Fe₂₀ film. \vec{B}_F of 3 nm Ni₈₀Fe₂₀ subjected to an out-of-plane magnetic field (\vec{B}_{\perp}) may be separated into two components. One field component is parallel or antiparallel to the \vec{B}_{\perp} direction and remains constant up to 140 nm from the Ni₈₀Fe₂₀ film. The other component is an inhomogeneous field parallel to the FM surface of which strength decreases steeply with increasing distance from the Ni₈₀Fe₂₀ electrode.

4. Materials and Methods

Materials

The donor molecules [mCP] and [MeO-TPD] and acceptor molecules [B3PYMPM] and [3TPYMB] were purchased from Lumtec Corporation. The Alq_3 molecule was purchased from Sigma-Aldrich. These materials were used 'as received' without further purification.

The OLEDs structure

The TADF-based OLEDs have an architecture of indium tin oxide (ITO)/poly(3,4-ethylenedioxythiophene):polystyrene sulfonate (PEDOT:PSS 40 nm)/mCP:B3PYMPM (40 nm, mCP:B3PYMPM=1:2)/LiF(1 nm)/Al(100 nm) or ITO/ PEDOT:PSS (40 nm)/mCP (4.5 nm)/mCP:B3PYMPM (27 nm, mCP:B3PYMPM=1:2)/B3PYMPM(9 nm)/LiF(1 nm)/Al(100 nm). The Alq₃ based OLEDs have the same structure where the active layer is replaced by different

thicknesses of Alq_3 films. The corresponding $Ni_{80}Fe_{20}$ or Co based OLEDs have an ferromagnetic layer between the LiF and aluminum layers.

The OLED Fabrication

The OLED devices were fabricated in a glovebox that has nitrogen atmosphere. The ITO anode substrate was cleaned by ultrasonic treatment with 2% micro-90 soap in deionized water (DI water), pure DI water, acetone, and isopropyl alcohol (IPA), each for 20 min. The PEDOT:PSS layer was spin-coated onto the ITO substrate, followed by an annealing treatment at 140 °C for 20 min. Subsequently the active layers were deposited using a thermal evaporation co-deposition system. Finally, the LiF, (NiFe or Co) and Al layers were deposited in another chamber in the same system. The active device area was 2mm x 2mm.

The MEL measurements

A positive bias voltage was applied to the ITO electrode of the OLED devices, which were placed in a vacuum cryostat with transparent windows. The EL emission was measured using a silicon detector. The device was placed between the two poles of an electromagnet that produced field strength, *B* up to 200 mT, which was applied parallel or perpendicular to the OLED surface. The B filed was swept at a speed of 10 mT/S from -200 mT to +200 mT and backward.

The VSM measurements

The samples were mounted on a quartz rod held by teflon tape between the electromagnet poles separated by 16 mm. The magnetic field was varied in the range of -200 mT - 200 mT at a step of 0.5 mT; or in the range of -1.5 T - 1.5 T at a step of 0.1 T.

Thickness measurements

The thickness of various films, active layers or FM substrates was estimated using Tencor P10 profilometer at the step edge of the film; he average of six consecutive measurements was taken to determine the film thickness.

AFM measurements

The film roughness was measured for the OLED device by a BrukerDimesion Icon atomic force microscope using scan-assist tapping mode with a nominal tip radius of 2 nm. The data was processed using NanoScope Analysis software.

MOKE measurement

Magnetic hysteresis loops were measured at room temperature by Sagnac MOKE, which has much higher sensitivity than conventional MOKE.²⁸

Supporting Information. Details experimental results (MEL responses) and device characterizations.

Corresponding Authors:

*E-mail:val@physics.utah.edu; o.kwon@samsung.com

Notes: The authors declare no competing financial interest.

Acknowledgements

12

We acknowledge Henna Popli for important comments. Support for this work was provided by the SAMSUNG Global Research Outreach (GRO) program (X.L.), the National Science Foundation grant DMR-1701427 (J.W.), and NSF EAGER grant DMR 1836989 (H.L.).

References

- (1) Xiong, Z.H., Wu, D., Vardeny, Z.V. and Shi, J., 2004. Giant Magnetoresistance in Organic Spin-valves. *Nature*, *427*(6977), p.821.
- (2) Sheng, P., Wang, B. and Li, R., 2018. Flexible Magnetic Thin Films and Devices. *Journal of Semiconductors*, 39(1), p.011006.
- (3) Fergen, I., Seemann, K., Weth, A.V.D. and Schüppen, A., 2002. Soft Ferromagnetic Thin Films for High Frequency Applications. *Journal of magnetism and magnetic materials*, 242, pp.146-151.
- (4) Caruso, M.J., Bratland, T., Smith, C.H. and Schneider, R., 1998. A New Perspective on Magnetic Field Sensing. *SENSORS-PETERBOROUGH-*, *15*, pp.34-47.
- (5) Nikitin, P.I., Valeiko, M.V., Toporov, A.Y., Ghorbanzadeh, A.M. and Beloglazov, A.A., 1998. Deposition of Thin Ferromagnetic Films for Application in Magnetic Sensor Microsystems. *Sensors and Actuators A: Physical*, *68*(1-3), pp.442-446.
- (6) Barmak, K. and Coffey, K. eds., 2014. *Metallic Films for Electronic, Optical and Magnetic Applications: Structure, Processing and Properties*. Woodhead Publishing.
- (7) Dumesnil, K. and Andrieu, S., 2012. Epitaxial Magnetic Layers Grown by MBE: Model Systems to Study the Physics in Nanomagnetism and Spintronic. *Molecular Beam Epitaxy: From Research to Mass Production*, p.487.
- (8) Wang, F., Macia, F., Wohlgenannt, M., Kent, A.D. and Flatté, M.E., 2012. Magnetic Fringe-field Control of Electronic Transport in an Organic Film. *Physical Review X*, 2(2), p.021013.
- (9) Bochi, G., Hug, H.J., Paul, D.I., Stiefel, B., Moser, A., Parashikov, I., Güntherodt, H.J. and O'Handley, R.C., 1995. Magnetic Domain Structure in Ultrathin Films. *Physical review letters*, 75(9), p.1839.
- (10) Hug, H.J., Stiefel, B., Moser, A., Parashikov, I., Klicznik, A., Lipp, D., Güntherodt, H.J., Bochi, G., Paul, D.I. and O'Handley, R.C., 1996. Magnetic Domain Structure in Ultrathin Cu/Ni/Cu/Si (001) Films. *Journal of applied physics*, *79*(8), pp.5609-5614.
- (11) Wang, F.J., Bässler, H. and Vardeny, Z.V., 2008. Magnetic Field Effects in π -conjugated Polymer-fullerene Blends: Evidence for Multiple Components. *Physical review letters*, 101(23), p.236805.
- (12) Devir-Wolfman, A.H., Khachatryan, B., Gautam, B.R., Tzabary, L., Keren, A., Tessler, N., Vardeny, Z.V. and Ehrenfreund, E., 2014. Short-lived Charge-transfer Excitons in Organic Photovoltaic Cells Studied by High-field Magneto-photocurrent. *Nature communications*, *5*, p.4529.
- (13) Zhang, C., Sun, D., Sheng, C.X., Zhai, Y.X., Mielczarek, K., Zakhidov, A. and Vardeny, Z.V., 2015. Magnetic Field Effects in Hybrid Perovskite Devices. *Nature Physics*, *11*(5), p.427.
- (14) Wang, Y., Sahin-Tiras, K., Harmon, N.J., Wohlgenannt, M. and Flatté, M.E., 2016. Immense Magnetic Response of Exciplex Light Emission due to Correlated Spin-charge Dynamics. *Physical Review X*, 6(1), p.011011.
- (15) Basel, T., Sun, D., Baniya, S., McLaughlin, R., Choi, H., Kwon, O. and Vardeny, Z.V., 2016. Magnetic Field Enhancement of Organic Light-emitting Diodes Based on Electron Donor—acceptor Exciplex. *Advanced Electronic Materials*, *2*(2), p.1500248.
- (16) Macia, F., Wang, F., Harmon, N.J., Kent, A.D., Wohlgenannt, M. and Flatté, M.E., 2014.

- Organic Magnetoelectroluminescence for Room Temperature Transduction between Magnetic and Optical Information. *Nature communications*, *5*, p.3609.
- (17) Harmon, N.J., Macià, F., Wang, F., Wohlgenannt, M., Kent, A.D. and Flatté, M.E., 2013. Including Fringe Fields from a nearby Ferromagnet in a Percolation Theory of Organic Magnetoresistance. *Physical Review B*, 87(12), p.121203.
- (18) Macia, F., Wang, F., Harmon, N.J., Wohlgenannt, M., Kent, A.D. and Flatté, M.E., 2013. Hysteretic Control of Organic Conductance due to Remanent Magnetic Fringe Fields. *Applied Physics Letters*, 102(4), p.042408.
- (19) Harmon, N.J., Wohlgenannt, M. and Flatté, M.E., 2016. Manipulation of the Electroluminescence of Organic Light-emitting Diodes via Fringe Fields from Patterned Magnetic Domains. *Applied Physics Letters*, 109(24), p.243303.
- (20) Cox, M., Kersten, S.P., Veerhoek, J.M., Bobbert, P. and Koopmans, B., 2015. Δ B Mechanism for Fringe-field Organic Magnetoresistance. *Physical Review B*, *91*(16), p.165205.
- (21) Sheng, Y., Nguyen, T.D., Veeraraghavan, G., Mermer, Ö., Wohlgenannt, M., Qiu, S. and Scherf, U., 2006. Hyperfine Interaction and Magnetoresistance in Organic Semiconductors. *Physical Review B*, 74(4), p.045213.
- (22) Kalinowski, J., Cocchi, M., Virgili, D., Di Marco, P. and Fattori, V., 2003. Magnetic Field Effects on Emission and Current in Alq3-based Electroluminescent Diodes. *Chemical Physics Letters*, *380*(5-6), pp.710-715.
- (23) Osada, K., Goushi, K., Kaji, H., Adachi, C., Ishii, H. and Noguchi, Y., 2018. Observation of Spontaneous Orientation Polarization in Evaporated Films of Organic Light-emitting Diode Materials. *Organic Electronics*, *58*, pp.313-317.
- (24) Baniya, S., Pang, Z., Sun, D., Zhai, Y., Kwon, O., Choi, H., Choi, B., Lee, S. and Vardeny, Z.V., 2016. Magnetic Field Effect in Organic Light-Emitting Diodes Based on Electron Donor–Acceptor Exciplex Chromophores Doped with Fluorescent Emitters. *Advanced Functional Materials*, *26*(38), pp.6930-6937.
- (25) Hu, B. and Wu, Y., 2007. Tuning Magnetoresistance between Positive and Negative Values in Organic Semiconductors. *Nature materials*, *6*(12), p.985.
- (26) Nguyen, T.D., Hukic-Markosian, G., Wang, F., Wojcik, L., Li, X.G., Ehrenfreund, E. and Vardeny, Z.V., 2010. Isotope Effect in Spin Response of π -conjugated Polymer Films and Devices. *Nature materials*, 9(4), p.345.
- (27) Yu, Z.G., Ding, F. and Wang, H., 2013. Hyperfine Interaction and its Effects on Spin Dynamics in Organic Solids. *Physical Review B*, 87(20), p.205446.
- (28) Liu, H., McLaughlin, R., Sun, D. and Vardeny, Z.V., 2018. Long-range Transverse Spin Seebeck Effect in Permalloy Stripes Using Sagnac Interferometer Microscopy. *Journal of Physics D: Applied Physics*, *51*(13), p.134003.